RESEARCH PAPER

Enhancing the design bending strength of new and aged glass with a functional coating

**Gregorio Mariggiò · Sara Dalle Vacche ·
Roberta Bongiovanni · Christian Louter ·
Mauro Corrado**

Abstract Annealed glass is susceptible to stress corrosion. This stress corrosion phenomenon, also known as static fatigue, embodies a reduction of the tensile strength due to the combined presence of applied tension stress and humidity. As a consequence, the effective strength of annealed glass members in building construction is limited. According to the classical theory developed to account for this phenomenology and to previous experiences published in the literature, stress corrosion can be prevented by avoiding the interaction between water molecules and the silica network. In the present work an innovative polymeric coating cured by UV radiation is applied to the surface of glass specimens to prevent stress corrosion. This coating is suitable to constitute a barrier between humidity and glass surface, thus increasing the reliability of new glass structures and their resistance to long-term loads, due to a compositional profile that maximizes hydrophobicity and water vapor barrier on the air side and adhesive properties on the substrate side. Coating effectiveness is assessed experimentally in terms of load-carrying capacity of coated plates tested under equibiaxial bending conditions with the coaxial double ring setup. New and naturally aged glasses are analyzed. The results evidence an increase of the design bending strength between 60 and 90% with respect to the strength of un-coated glass.

Keywords Annealed glass · Stress corrosion · Bending strength · Polymeric coating · UV-curing technology

G. Mariggiò · M. Corrado (✉)
Department of Structural, Geothecnical and Building Engineering, Politecnico di Torino, Corso Duca degli Abruzzi 24, 10129 Turin, Italy
e-mail: mauro.corrado@polito.it

G. Mariggiò
e-mail: gregorio.mariggio@polito.it

S. Dalle Vacche · R. Bongiovanni
Department of Applied Science and Technology, Politecnico di Torino, Corso Duca degli Abruzzi 24, 10129 Turin, Italy
e-mail: sara.dallevacche@polito.it

R. Bongiovanni
e-mail: roberta.bongiovanni@polito.it

C. Louter
Institute of Building Construction, Technische Universität Dresden, August-Bebel-Straße 30, 01219 Dresden, Germany
e-mail: christian.louter@tu-dresden.de
URL: http://www.bauko.bau.tu-dresden.de

1 Introduction

The use of glass in the building industry is evolving towards structural applications: modern architecture features large glass facades, all-glass staircases, roofs, walkways and spectacular long suspended bridges. In the last decade an intense research activity has brought to the development of new structural elements such as, among others, bricks, post-tensioned laminated beams, sandwich structures with thin and ultra-

thin glass panes, and new recipes, thus fostering the use of glass for structural components. High compressive strength, exceeding 200 MPa (Haldimann et al. 2008), and transparency are the most attractive properties of glass from the structural and the architectural point of view. However, the almost perfect elastic-brittle mechanical response and the sensitivity to cracking make glass a challenging building material. Glass has an extremely variable exploitable tensile strength, which can reach values in the range of 200–500 MPa (Jotz et al. 2018), depending on the size of surface flaws and the presence of chemical or thermal treatments. Aiming at increasing the reliability of glass as structural material, nowadays, several aspects of the tensile strength are still object of study: the relation between the size of surface flaws and the strength (Abrams and Green 2006; Overend et al. 2007; Overend and Zammit 2012), the effect of ageing (Afolabi et al. 2016; Datsiou and Overend 2017a, b), the effectiveness of repairs on strength recovery (Overend and Louter 2015), and the derivation of the best statistical distribution function for the strength to be included in the probabilistic approach for structural design (Pisano and Royer Carfagni 2015; Kinsella and Persson 2018). Besides the problem of surface flaws, another chemical-physical phenomenon limits the exploitation of the intrinsic tensile strength of annealed glass and does not allow to apply high long-term loads: the stress corrosion.

The stress corrosion phenomenon, also known as static fatigue, consists in a reduction of the material strength caused by the combined action of applied stress and humidity on the silica network that composes glass. The classical theory to account for this phenomenology involves the chemical reaction of water molecules with the silica network, taking place at the tip of the cracks, although other interpretations have been also provided (Gy 2003).

Static fatigue in glass was discovered at the end of the nineteenth century by Grenet (1899), who observed that the strength of glass depended on the rate of loading or on the length of time a load was applied. However, only in the 1960s' a clear explanation was found for this phenomenon. In that decade, several experimental tests were carried out that permitted to identify different stages of crack propagation in glass and to measure the effects of water and water vapor on the sub-critical propagation of microcracks (Wiederhorn 1967; Wiederhorn and Bolz 1967). As represented by the schematic representation shown in Fig. 1, there is a
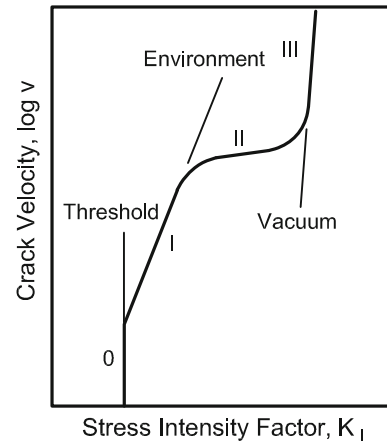

Fig. 1 Velocity of a running crack versus strain energy release rate. Adapted from Lawn (1993)

threshold for the applied stress, here represented by the stress intensity factor, below which crack propagation does not occur, even in the sub-critical regime. Once the threshold is overcome, three regions are evidenced for crack propagation velocity. In region I the crack velocity is dependent on the applied stress; in region II the crack velocity is nearly independent of the applied stress; in region III the crack velocity is again function of the applied stress, however, the slope is very high, relating to an unstable crack propagation that occurs when the stress intensity factor overcomes the material toughness, $K_I > K_{IC}$. The stress corrosion occurs in regions I and II that, in fact, are highly influenced by the amount of environmental humidity.

Pioneering experimental studies carried out by Wiederhorn (1967) allowed to derive empirical relationships between the sub-critical crack propagation velocity and the stress field –represented by the stress intensity factor at the crack tip– for different percentages of environmental humidity (see Fig. 2). According to Fig. 2 the effect of an increasing amount of water in the environment is a shift of region I towards lower values of K_I, without changing the slope, and a shift of region II towards higher values of crack velocity.

Charles and Hillig (1962) first proposed a theory based on chemical reactions to explain the phenomenon of stress corrosion. Then, 20 years later, Michalske and Freiman (1983), starting from the phenomenological model proposed by Charles and Hillig developed a detailed chemical model for the interaction of the environment with mechanically strained bonds in glass at the crack tip. The reaction involves three steps, as rep-
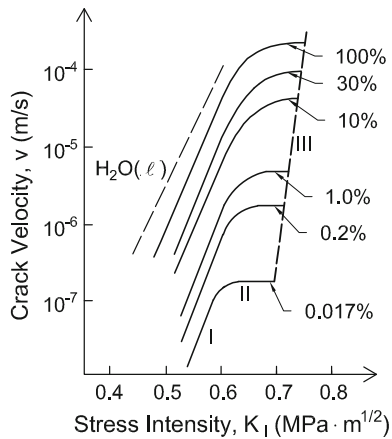
Fig. 2 Effect of humidity on the crack propagation in soda-lime glass. Adapted from Wiederhorn (1967)

resented in Fig. 3a: (i) a water molecule from the environment approaches a bridging Si–O–Si bond at the crack tip, and forms an hydrogen bond with the oxygen atom belonging to the silica network (here indicated with O_{br}) while the lonepair orbitals from the oxygen of water (here indicated with O_w) interact with the Si atom; (ii) a proton transfer to O_{br} and an electron transfer from O_w to the Si atom occur with a concerted reaction, resulting in the destruction of the original bridging bond between O_{br} and Si, and in the formation of two new bonds: one between O_w and Si, and one between H and O_{br}; (iii) finally, the bond between O_w and transferred H breaks. As a result, surface hydroxyl groups are now present on each fracture surface. The chemical process is enhanced by the presence of alkali ions, like in the case of soda-lime silica glass (Ronchetti et al. 2013). In this case, the presence of terminal structures, in which sodium alkali ions are associated to the very strong Si–O–Si unending network through an oxygen–sodium ionic bond, strongly influences the reaction at the crack tip between soda-lime glass and water molecules. As a first step in fact, the oxygen–sodium bond breaks down, and the oxygen dissociates the water molecule to satisfy its force field with a hydrogen ion or a free hydroxyl ion. This facilitates the occurring of the second step, in which the strong bond between silicon and oxygen breaks, yielding two ends: one end becomes a silanol end by attachment of the hydroxide ion or by proton transfer while on the other end a new terminal structure is formed, capable of dissociating another water molecule (see Fig. 3b).

Stress corrosion, as any other chemical reaction, is an activated process. The activation energy is provided

by mechanical stress and, therefore, the reaction occurs more rapidly where the stress field is the largest, i.e., at the tip of micro-cracks (Michalske and Freiman 1983).

Solutions to such a problem proposed in the literature include, among others: polymeric and metallic coatings for glass rods and silica lightguides (Bouten 1987; Kurkjian et al. 1993; Chen et al. 1995), silicon grease for the edge strengthening of glass plates (Lindqvist et al. 2012), and graphene coatings (Wang et al. 2016).

In this work, the performance of a functional coating recently developed by the present authors in preventing glass stress corrosion is examined. The coating is characterized by a compositional profile aiming at combining hydrophobicity and barrier to water vapor with good adhesion to glass. Such a goal was achieved by developing an UV-curable acrylic system copolymerized with a methacrylic perfluoropolyether and an acrylic silane (Dalle Vacche et al. 2019b). The challenge was to obtain the best balance between hydrophobicity and adhesion of the coating, which are usually in competition. The composition of the coating was thus chosen aiming at developing a copolymer exhibiting a compositional gradient, so that the obtained coating ensured water repellency thanks to the surface segregation of the fluorinated component, and adhesion towards the glass substrate, thanks to the presence of the silane at the interface.

In Sect. 2 of the present paper the procedures to produce and apply the polymeric resin are outlined and the main physical-mechanical properties of the obtained coating are reported. Then, Sect. 3 concerns the assessment of the coating effectiveness in stress corrosion prevention on new and naturally aged glasses, by means of mechanical tests on un-coated and coated specimens. Finally, in Sect. 4 the analysis of the experimental results based on Weibull statistics is reported, together with a clear quantification of the improvement consequent to the application of the coating.

2 Compositionally graded coating

A polymeric coating was prepared using an UV-curable formulation, based on a hydrocarbon acrylic resin (Ebecryl® 130, by Allnex Belgium SA, Drogenbos, Belgium) and a photoinitiator (Darocur® 1173, by BASF, Germany), added with a small amount (1 phr) of a fluorinated methacrylate (Fluorolink® MD700, by

Fig. 3 Representation of the reaction between water and strained Si–O–Si bond at the crack tip: **a** silica glass; **b** soda-lime silica glass

(a)   **(b)**
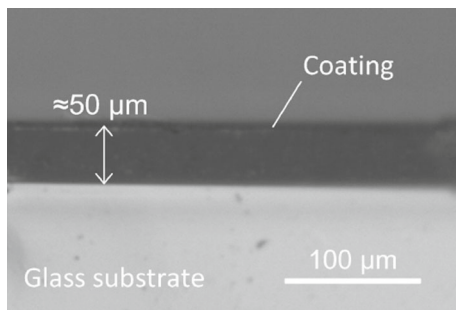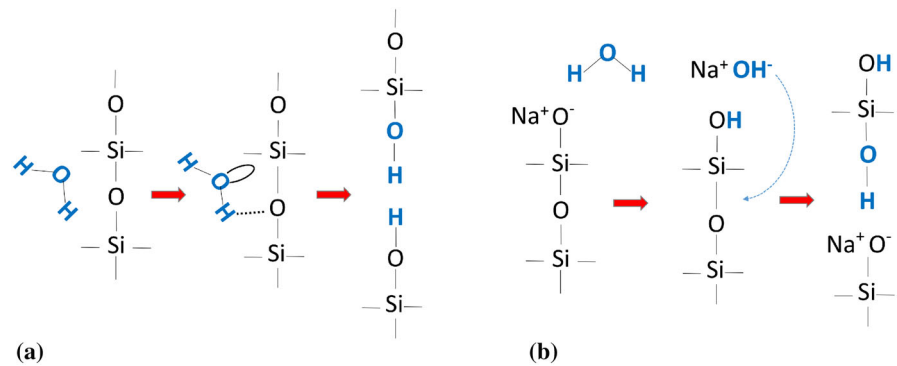
Fig. 4 Cured coating on the glass substrate

Solvay Specialty Polymers, Bollate Milano, Italy). The formulation, whose details can be found in Dalle Vacche et al. (2019b), was coated on glass, previously treated with a silane primer containing an acrylic group (3-(acryloyloxy) propyltrimethoxysilane, Alfa Aesar by Thermo Fisher (Kandel) GmbH, Karlsruhe, Germany). The primer modifies the glass surface by reaction with the silanol groups, while through the acrylic functions it co-reacts with the (meth)acrylic resins upon UV irradiation. Forming covalent bonds between the soda-lime glass and the coating, it increases the adhesion strength. In the case discussed in this article, the silylation of the glass was performed by immersing the specimens in solutions of the silane in water (0.2 vol%) for 5 min at room temperature, rinsing them with deionized water and drying them in an oven at 100 °C for 30 min to facilitate silanol condensation. The coating was spread on the glass surface by a wire wound bar, and cured by UV irradiation, according to the procedure reported in Dalle Vacche et al. (2019b). After irradiation a transparent solid film, with a thickness of 50 μm, as revealed by inspection with an optical microscope and shown in Fig. 4, was obtained.

The formulation here described was chosen to provide a compositionally graded coating able to ensure within one layer good barrier to water vapor, hydrophobicity, transparency and adhesion properties, as needed for hindering the stress corrosion of glass. The hydrocarbon resin is transparent and has acceptably low water vapour transmission rate ($WVTR_{25}$), however it is not water repellent, as shown by the water contact angle θ_{water} which is lower than 90°. The fluorinated resin has high water repellency (water contact angle θ_{water} higher than 90°), but has high permeability, and shows poor adhesion strength (τ). The properties of the resins and of the compositionally graded coating were studied in previous works (Dalle Vacche et al. 2019a, b), and are summarized in Table 1 for convenience.

As discussed in Vitale et al. (2013, 2015) and Bongiovanni et al. (1998), adding a small amount of a fluorinated resin to a hydrocarbon resin results in a compositional gradient as sketched in Fig. 5: due to the difference in polarity between the two resins, the fluorinated one selectively migrates to the air surface and is not present at the glass interface. This gradient becomes irreversible after curing under UV light the latter. Therefore, the coating shows the water repellency of the fluorinated component, although it is present at low concentration; the adhesion and water vapour transmission rate are not affected as these properties are imparted by the hydrocarbon resin covalently linked to the silane primer at the glass interface.

3 Assessment of the effectiveness of the coating

3.1 Coaxial double ring test

The effectiveness of the coating in protecting glass surfaces against stress corrosion was assessed experimentally by comparing the load-carrying capacity of

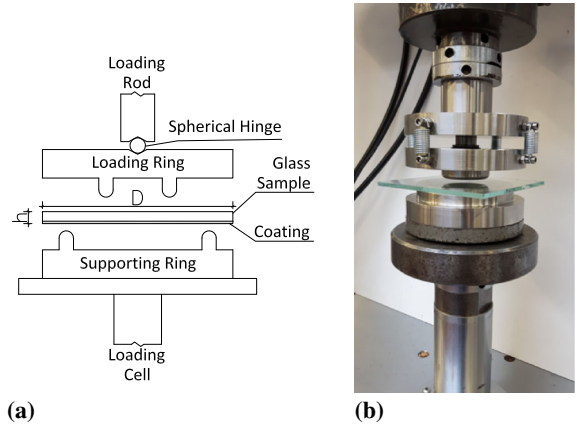**Table 1** Properties of the coating and of its components

Composition	WVTR$_{25}$ (g/m^2/24h)	θ_{water} (°)	Adhesion strength τ (MPa)
Compositionally graded coating	87.1 ± 15.8	103.2 ± 1.6	24.9 ± 2.8
Hydrocarbon acrylate resin	53.1 ± 7.8	67.6 ± 4.1	24.5 ± 2.8
Fluorinated methacrylate	316.0 ± 20.2	102.9 ± 2.6	5.8 ± 1.0
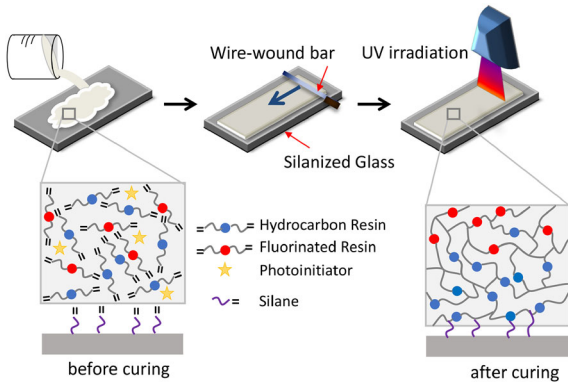
Fig. 5 Schematic representation of the compositionally graded coating

Fig. 6 Coaxial double ring set-up

coated and un-coated specimens. Equibiaxial bending tests were carried out with a coaxial double ring setup having the supporting ring with diameter $D_S = 90$ mm and the loading ring with diameter $D_L = 40$ mm (see Fig. 6). Square glass samples were tested, having nominal thickness $h = 4$ mm and edge size $l = 120$ mm. The dimensions of the testing rig and the samples, and their ratios were designed according to the prescriptions provided by the ASTM C1499-09 Standard (ASTM C1499–09 2013), in line with a number of similar experiments recently carried out to investigate the bending strength of glass (Overend and Louter 2015; Datsiou and Overend 2017a, 2018). A servo-hydraulic MTS universal testing machine was used, with a load cell capacity of 10 kN. The loading ring was connected to the testing machine with an articulated joint to ensure uniform contact between the loading ring and the surface of the specimen.

Four typologies of glass samples were tested: (i) new un-coated glass samples (NU), (ii) new coated glass samples (NC), (iii) naturally aged un-coated glass samples (AU), (iv) naturally aged coated glass samples (AC). Sets of 25 and 20 specimens were tested for un-coated and coated glass, respectively. To ensure constant and harsh environmental conditions for stress

corrosion, the supporting ring and the specimens were inserted in a watertight container filled with water, for the entire duration of the test. The pH of the water was monitored and the water was replaced whenever its pH deviated from the neutral value to avoid any effect on the reaction between water molecules and glass.

Both new and aged glasses were soda-lime glass, as proven by the FTIR-ATR (Fourier Transform InfraRed-Attenuated Total Reflection) spectroscopy carried out on selected samples and shown in Fig. 7. Peaks of the absorbance at 910 cm^{-1} and 768 cm^{-1} are representative of the symmetric and asymmetric vibration of the Si–O–Si bond (Amma et al. 2015). The IR spectra of the new and aged glasses used in this study are compared to that of a microscope slide made of low-iron soda-lime glass. All the three spectra shown in Fig. 7 are perfectly overlapped.

Concerning the ageing conditions of the naturally aged glass samples, they were cut from glass panes of single glazing windows obtained from refurbishment works of a low-rise building located in Torino, Italy. Their service life was between 25 and 30 years. Since we had no information on which side was exposed to weather, we inspected both sides of the glass panes
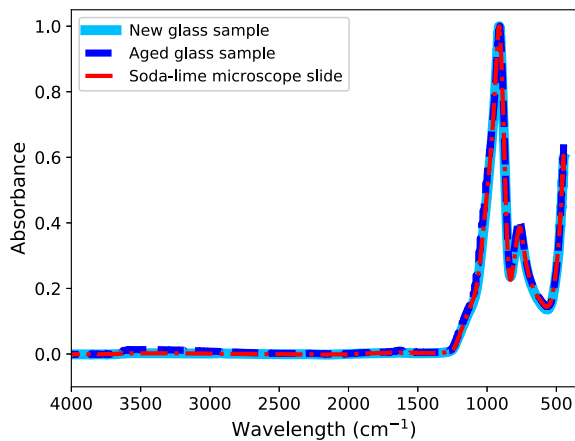
Fig. 7 FTIR-ATR spectra of new and aged glasses, compared to that of a reference soda-lime glass

$$\sigma_f = \frac{3F}{2\pi h^2}\left[(1-\nu)\frac{D_S^2 - D_L^2}{2D^2} + (1+\nu)ln\frac{D_S}{D_L}\right] \quad (1)$$

where F is the failure load, h is the nominal thickness of the specimen, D_S and D_L are the diameters of the supporting and loading rings, respectively, D is the diameter of the glass specimen, and $\nu = 0.22$ is the Poisson's ratio of glass. For a rectangular test specimen, D is the diameter of a circle that expresses the characteristic size of the plate as follows:

$$D = \frac{l}{0.90961 + 0.12652\frac{h}{D_S} - 0.00168 ln\frac{l-D_S}{h}} \quad (2)$$

where

$$l = 0.5(l_1 + l_2) \quad (3)$$

and l_1 and l_2 are the lengths of the edges.

3.2 Statistical analysis of strength data

The statistical distribution of the glass strength, σ_f, can be represented by a two parameter Weibull distribution function:

$$P_f = 1 - \exp\left[-\left(\frac{\sigma_f}{\theta}\right)^\beta\right] \quad (4)$$

where P_f is the cumulative distribution function of failure, and β and θ are the Weibull shape and scale parameters, obtained by the best-fitting of experimental data. The Weibull distribution function can be linearized by taking the logarithm twice:

$$\ln\left(\ln\left(\frac{1}{1-P_f}\right)\right) = \beta\ln(\sigma_f) - \beta\ln(\theta) \quad (5)$$

According to EN 12603 (2002), β and θ parameters were calculated with the good linear unbiased estimators method:

$$\hat{\beta} = \frac{nk_n}{\frac{s}{n-s}\sum_{i=s+1}^{n}\ln\sigma_i - \sum_{i=1}^{s}\ln\sigma_i} \quad (6)$$

$$\hat{\theta} = \exp\left[\frac{1}{n}\sum_{i=1}^{n}\ln\sigma_i + 0.5772\frac{1}{\hat{\beta}}\right] \quad (7)$$

where n is the sample size, s is the largest integer less than $0.84n$, and the values of k_n, estimated as a function of the sample size n, are listed in Table 3 of EN 12603 (2002).

Strength data, σ_f, were ranked in ascending order ($i = 1$ to n) to build an Ordered Sample. Then, a prob-

by means of an optical microscope looking for differences in the surface deterioration. No evident differences were observed in terms of size and shape of flaws and scratches. Therefore, for both new and aged specimens the same criterion was used to choose the surface of the specimen to be tested, which is the one put in tension during the bending test: we chose to test the side exposed to air during the production of the glass panes. Consistently, the coating was applied on the air side in all the cases, while a self-adhesive film was applied on the tin side in order to hold the fragments together after breaking of the specimen.

The loading tests were carried out under displacement control. Two series of tests were carried out on the un-coated specimens: one with a low displacement rate, equal to 0.7 μm/s, which corresponds to a stress rate of 0.15 MPa/s, and the other one with a high displacement rate, equal to 14.0 μm/s, which corresponds to a stress rate of 3.0 MPa/s. The low rate caused fracture of the samples within 600–900 s, whereas the high rate within 30–50 s. Therefore, the specimens tested at the high displacement rate are only slightly affected by stress corrosion, as reported in the literature (Lindqvist et al. 2012), while remaining in the quasi-static regime. It is worth noting that the effects of stress corrosion are negligible only with higher stress rates, which approach the dynamic regime (Haldimann 2006). The coated specimens were tested only at the low displacement rate.

The equibiaxial strength, σ_f, was calculated from the failure load, F, by means of the following equation, provided by ASTM C1499-09 (2013):

ability of failure was assigned to each value σ_i of the Ordered Sample by means of probability estimators $\hat{G}_i$:

$$\hat{G}_i = \frac{i - 0.3}{n + 0.4} \qquad (8)$$

Finally, each point $(\sigma_f, \hat{G}_i)$ was plotted into the Weibull diagram, which relates the probability of failure (%) to the failure stress (MPa).
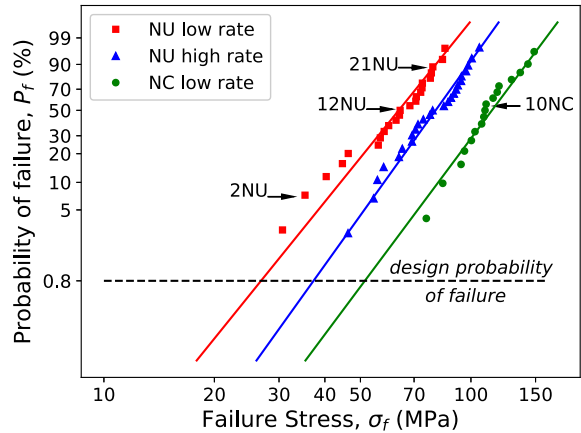
4 Results and discussion

4.1 Probability of failure

The Weibull diagrams for new and aged un-coated specimens tested at low stress rate (0.15 MPa/s) are shown in Fig. 8. Both sets of data are well fitted by a straight line, proving that they can be appropriately interpreted with the Weibull statistics. The curve that best fit the data points of AU specimens (rhombus markers) is characterized by $\hat{\beta} = 5.3$ and $\hat{\theta} = 46.8$ MPa, while that for NU specimens (square markers) has $\hat{\beta} = 5.2$ and $\hat{\theta} = 68.3$ MPa. As expected, the parameter $\hat{\beta}$, which represents the slope of the linearized Weibull diagram and therefore is indicative of the strength scatter, is almost the same for new and aged glass. The obtained values are within the range of values reported in the literature for flat glass, namely 3–7 (Le Bourhis 2014). On the contrary, the parameter $\hat{\theta}$, which is the strength associated to a probability of failure of 63.2%, is lower in the case of aged glass, because of the pres-
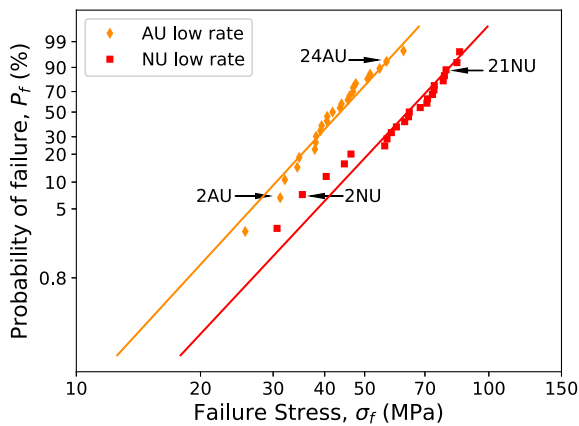
Fig. 9 Weibull distribution function of the probability of failure for coated (NC) and un-coated (NU) new glass samples. The specimens subjected to microscopy inspection after the test are identified by a label

ence of larger surface defects. Graphically, the increase of strength is represented by a shift of the curve towards higher values of failure stress.

The Weibull diagrams for new un-coated specimens tested at low and high stress rates, and for new coated specimens tested at low stress rate are shown in Fig. 9. Again, all the three sets of data are well fitted by the Weibull distribution function. The increase of the imposed stress rate reduces the effect of the stress corrosion, thus leading to a shift of the data points toward higher values of strength (triangles). Such a strengthening effect can be clearly quantified by the parameter $\hat{\theta}$, which increases from 68.3 MPa to 85.3 MPa. The effectiveness of the developed coating in preventing stress corrosion is evident from the results shown in Fig. 9. The set of points representing the probability of failure of NC specimens at low stress rate (circles) is the most shifted rightwards, being characterized by $\hat{\theta} = 121.8$ MPa. The parameter $\hat{\beta}$ has very similar values in the three cases. In the same diagram a horizontal dashed line is drawn to indicate the probability $P_f = 0.8\%$, which corresponds to a commonly used probability of failure for glass design (Beason and Morgan 1985). By extrapolating the experimental data points through the best fitting Weibull distribution functions, the following design bending strengths are obtained: 26.8 MPa for NU low rate specimens, 37.3 MPa for NU high rate specimens, and 51.4 MPa for NC specimens. Therefore, we can conclude that the coating allows to increase of about 92% the design bending strength.
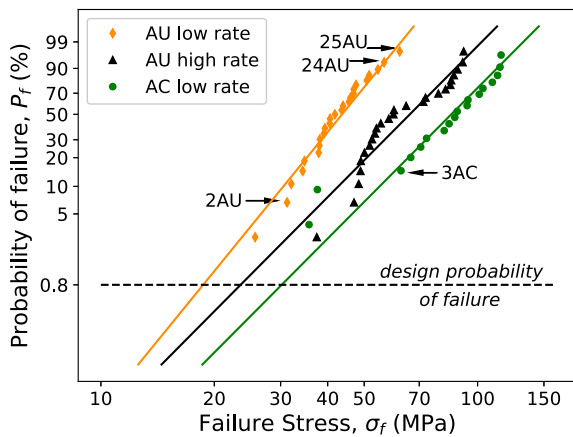

Fig. 8 Weibull distribution function of the probability of failure for new (NU) and naturally aged (AU) un-coated glass samples tested at low stress rate. The specimens subjected to microscopy inspection after the test are identified by a label

Fig. 10 Weibull distribution function of the probability of failure for coated (AC) and un-coated (AU) naturally aged glass samples. The specimens subjected to microscopy inspection after the test are identified by a label

Very similar results were obtained in the case of naturally aged glass specimens. The Weibull diagrams for aged un-coated specimens tested at low and high stress rates, and for aged coated specimens tested at low stress rate are shown in Fig. 10. The data points referred to AU low rate and AC sets of specimens are well approximated by the Weibull distribution, except for two points of the set AC, which are out of trend, whereas the results of the set AU high rate are more departed from the straight line representative of the Weibull distribution. As obtained in the case of new glass specimens, the un-coated aged glass tested at low stress rate exhibited the lowest strength, $\hat{\theta} = 46.8$ MPa, followed by the un-coated aged glass tested at high stress rate, $\hat{\theta} = 72.0$ MPa, and the coated specimens, $\hat{\theta} = 92.7$ MPa. With reference to the design probability of failure of 0.8%, the application of the coating to aged glass leads to an increase of the design bending strength of about 62%, being the design strength of coated glass equal to 30.2 MPa, and that of un-coated glass equal to 18.7 MPa.

All the results of the statistical analysis carried out on the experimental data are summarized in Table 2. They include, for each series of tests, the number of specimens that failed in an acceptable way, the Weibull shape parameter $\hat{\beta}$, the Weibull scale parameter $\hat{\theta}$, the coefficient of variation $\hat{CV}$, and the design bending strength $\hat{\sigma}_{\mathrm{f},0.008}$.[1]

---

[1] The Weibull parameters and the design bending strength values are not statistically indistinguishable and are within the 95% confidence levels of each other for sample sizes of 20 or 25.

4.2 Microscopy inspection

After each test, the crack pattern was carefully analyzed by naked eye to identify the position of the flaw that caused the specimen failure (see, for example, Figs. 11a and 12a, where the critical flaw is pinpointed by a black arrow) and to discard possible invalid tests, i.e., those with origin of failure located outside the loading ring. Moreover, an inspection with an optical stereo microscope Nikon SMZ18 was carried out on selected specimens to investigate the relation between flaw size and failure stress and the effect of the coating. Starting from the identification of the likely origin of failure (Fig. 11a), a first magnification of the lateral face of the fragment has permitted to identify the different regions of crack propagation that develop around the origin, i.e., mirror, mist and hackle zones, and Wallner lines (Fig. 11b). Finally, a further magnification permitted to reveal and measure the size of the critical flaw (Fig. 11c).

The microscopy inspections shown in Figs. 11 and 12 refer to a new un-coated specimen, identified with the id. number 21NU, and an aged un-coated specimen, identified with the id. number 24AU, respectively. These two specimens had the same kind of critical defect, namely a pit, and a similar probability of failure, being $P_f = 88.5\%$ for 21NU and $P_f = 93.3\%$ for 24AU (see Fig. 8). However, different values of failure stress, $\sigma_f = 78.7$ MPa for 21NU and $\sigma_f = 56.5$ MPa for 24 AU, correspond to the same probability of failure because of a different distribution of defect size for new and aged glasses. In fact, the depth of the critical flaw is about 35 μm for specimen 21NU and 60 μm for specimen 24AU. In this case, the difference in the failure stress can be easily interpreted on the base of the relationship between failure stress and crack size derived from linear elastic fracture mechanics:

$$\sigma_{\mathrm{f}} = \frac{K_{IC}}{Y\sqrt{\pi a}}, \tag{9}$$

where Y is a geometry and loading factor, a is the crack depth, and K_{IC} is the fracture toughness. For the two cases we are examining, by assuming $K_{IC} = 0.75$ MPa m$^{\frac{1}{2}}$ and $Y = 0.94$ (which is between $Y = 0.71$, which holds for half-penny shaped cracks, and $Y = 1.12$, which holds for straight-fronted edge cracks in a semi-infinite solid (Overend and Zammit 2012)), Eq. (9) provides $\sigma_f = 76.1$ MPa for specimen 21NU and

Table 2 Statistical data of the experimental results

Id. code	Type of glass	Coating	Loading rate (MPa/s)	No. of valid specimens	Weibull param. $\hat{\beta}$	Weibull param. $\hat{\theta}$ (MPa)	$\hat{CV}$ (%)	$\hat{\sigma}_{f,0.008}$ (MPa)
NU low rate	New	Un-coated	0.15	23	5.2	68.3	24.2	26.8
NU high rate	New	Un-coated	3.00	25	5.8	85.3	20.6	37.3
NC low rate	New	Coated	0.15	18	5.6	121.8	17.7	51.4
AU low rate	Aged	Un-coated	0.15	25	5.3	46.8	19.6	18.7
AU high rate	Aged	Un-coated	3.00	25	4.3	72.0	25.7	23.4
AC low rate	Aged	Coated	0.15	18	4.3	92.7	28.2	30.2

Fig. 11 Fractography of sample 21NU, $\sigma_f = 78.7$ MPa: **a** location of the likely origin of failure; **b** mirror, mist and hackle zones, Wallner lines; **c** critical flaw
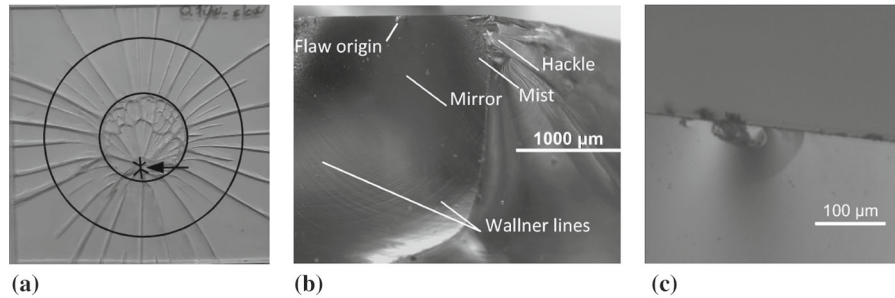

Fig. 12 Fractography of sample 24AU, $\sigma_f = 56.5$ MPa: **a** location of the likely origin of failure; **b** mirror and mist zones, Wallner lines; **c** critical flaw
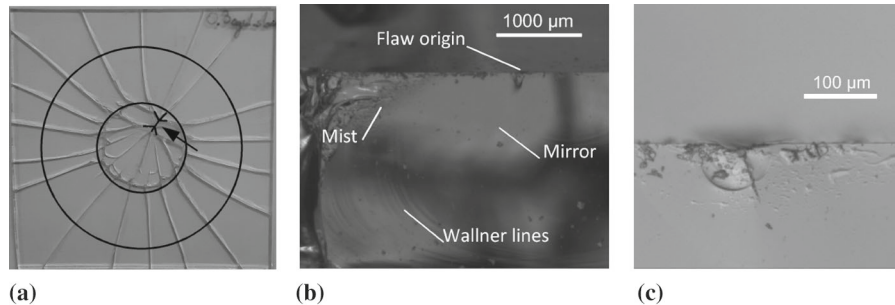
$\sigma_f = 58.1$ MPa for specimen 24AU. These two values are very close to the experimental ones.

The critical flaws shown in Fig. 13 refer again to two un-coated specimens, namely 2NU and 2AU, which have a similar probability of failure, placed on the left tail of the Weibull diagram (see Fig. 8). In this case, the two defects have a similar depth, equal to about 100 μm, although a different shape: the specimen 2NU has a pit, whereas the specimen 2AU has a scratch.

The pictures shown in Fig. 14 allow to compare the critical flaw of an aged un-coated specimen, 25AU, with that of an aged coated specimen, 3AC. The two samples have critical flaws with the same shape –half-penny shape– and depth equal to about 50 μm. Both failed under a bending stress of about 62 MPa. The crit-
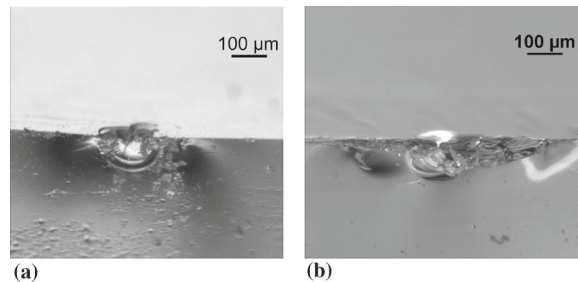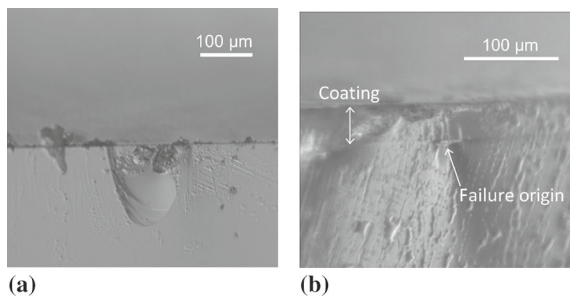

Fig. 13 Critical flaw: **a** sample 2NU, $\sigma_f = 35.3$ MPa; **b** sample 2AU, $\sigma_f = 31.2$ MPa

ical flaw of specimen 25AU is the smallest we found for the set of aged un-coated specimens, whereas that of specimen 3AC is one of the largest within the set of aged
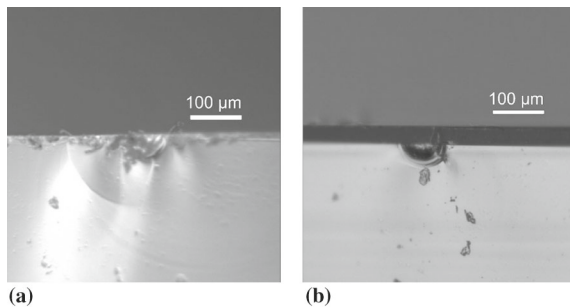
Fig. 14 Critical flaw: **a** sample 25AU, $\sigma_f = 62.1$ MPa; **b** sample 3AC, $\sigma_f = 62.6$ MPa

Fig. 15 Critical flaw: **a** sample 12NU, $\sigma_f = 64.1$ MPa; **b** sample 10NC, $\sigma_f = 110.0$ MPa

coated specimens (see Fig. 10). Since un-coated and coated samples belonged to the same set of aged glass panes, and there was no reason for having larger defects in un-coated samples, we can infer that the original critical flaw in specimen 25AU was smaller than that in specimen 3AC and it grew during the test because of stress corrosion up to the size shown in Fig. 14a. Moreover, since defects with the same shape and size gave the same failure stress in un-coated and coated conditions, we may suppose that the coating does not exert any mechanical strengthening. However, such a conclusion cannot be drawn based on only two specimens. A final statement on this aspect would require further investigations, which include also the comparison of the bending stiffness of un-coated and coated specimens.

Furthermore, in Fig. 14a the semi-elliptical line typical of a slow crack growth (Michalske et al. 1981; Michalske 1984; Quinn 2016) is clearly visible.

Finally, Fig. 15 shows the critical flaw of a new un-coated specimen, 12NU, and that of a new coated specimen, 10NC. The failure stress of such samples is close to the mean strength ($P_f = 50\%$) of the corresponding

set of specimens. The size of the two defects is very different, thus confirming the effectiveness of the coating in inhibiting stress corrosion.

5 Conclusions

A polymeric coating prepared with an UV-curable resin, a fluorinated methacrylate co-monomer, and a co-reactive silane primer to provide a good barrier to water vapor, hydrophobicity, transparency and adhesion properties has been tested as a barrier layer to prevent glass stress corrosion. Its performance has been assessed by comparing the failure stress of un-coated and coated specimens, tested with the coaxial double ring setup. The results reported in Sect. 4 prove that the proposed formulation is highly effective for both new and naturally aged glass. The increase of the bending strength corresponding to a probability of failure of 0.8% is equal to 92% for new glass and 62% for aged glass. Besides the very good performance against stress corrosion, the developed coating has some advantages compared to other strengthening techniques and coatings: it is solvent free, it has a very fast curing time, it is low-energy consuming, and it can be easily included in the continuous production systems of flat glass as well as it is available for in-situ applications.

While the effectiveness of the coating in preventing stress corrosion within few days after its application on the glass substrate has been proven, its durability remains to be investigated. In this context, three scenarios are foreseen: (i) artificial weathering carried out by exposing coated specimens to fluorescent UV lamps, heat and water, following standardized cycles such as those proposed by EN ISO 16474–3:2013 (2013); (ii) artificial ageing by means of sand abrasion to simulate the effect of impacts and scratches during the service life of the glass structures (Datsiou and Overend 2017a); (iii) mechanical ageing by subjecting coated samples to cyclic loads in order to stress repeatedly the coating and evaluate the appearance of possible microcracking in the coating that can reduce the water vapor barrier effect.

chi from Cromology Italia S.p.A. for their active contribution to the project GLASS & CO.

Compliance with ethical standards

Conflict of interest The authors declare that they have no conflict of interest.

References

Abrams, M.B., Green, D.J.: Prediction of crack propagation and fracture in residually stressed glass as a function of the stress profile and flaw size distribution. J. Eur. Ceram. Soc. **26**, 2677–2684 (2006)

Afolabi, B., Scott Norville, H., Morse, S.M.: Experimental study of weathered tempered glass plates from the Northeastern United States. ASCE J. Archit. Eng. **22**, 04016010 (2016)

Amma, S., Luo, J., Pantano, C.G., Kim, S.H.: Specular reflectance (SR) and attenuated total reflectance (ATR) infrared (IR) spectroscopy of transparent flat glass surfaces: a case study for soda lime float glass. J. Non Cryst. Solids **428**, 189–196 (2015)

ASTM C1499-09. Standard Test Method for Monotonic Equibiaxial Flexural Strength of Advanced Ceramics at Ambient Temperature. ASTM International, West Conshohocken (USA) (2013)

Beason, W.L., Morgan, J.R.: Glass failure prediction model. J. Struct. Eng. **111**, 2058–2059 (1985)

Bongiovanni, R., Malucelli, G., Pollicino, A., Tonelli, C., Simeone, G., Priola, A.: Perfluoropolyether structures as surface modifying agents of UV-curable systems. Macromol. Chem. Phys. **199**, 1099–1105 (1998)

Bouten, P.C.P.: Lifetime of Pristine Optical Fibres. Technische Universiteit Eindhoven, Eindhoven (1987)

Charles, R.J., Hillig, W.B.: The kinetics of glass failure by stress-corrosion. In: Symposium on Mechanical Strength of Glass and Ways of Improving It. Union Scientifique Continentale du Verre, Charleroi, Belgium, pp. 511–527 (1962)

Chen, X.M., Ellis, B., Wang, F., Seddon, A.B.: Strengthening of glass rods with ormosil polymeric coatings. J. Non Cryst. Solids **185**, 1–17 (1995)

Dalle Vacche, S., Forzano, S., Vitale, A., Corrado, M., Bongiovanni, R.: Glass lap joints with UV-cured adhesives: use of a perfluoropolyether methacrylic resin in the presence of an acrylic silane coupling agent. Int. J. Adhes. Adhes. **92**, 16–22 (2019a)

Dalle Vacche, S., Mariggiò, G., Vitale, A., Bongiovanni, R., Corrado, M.: Compositionally graded hydrophobic UV-cured coatings for the prevention of glass stress corrosion. Coatings **9**, 424 (2019b)

Datsiou, K.C., Overend, M.: Artificial ageing of glass with sand abrasion. Constr. Build. Mater. **142**, 536–551 (2017a)

Datsiou, K.C., Overend, M.: The strength of aged glass. Glass Struct. Eng. **2**, 105–120 (2017b)

Datsiou, K.C., Overend, M.: Weibull parameter estimation and goodness-of-fit for glass strength data. Struct. Saf. **73**, 29–41 (2018)

EN 12603:2002. Glass in building—procedures for goodness of fit and confidence intervals for Weibull distributed glass strength data. European Committee for Standardization, Brussels (2002)

EN ISO 16474-3:2013. Paints and varnishes—methods of exposure to laboratory light sources. European Committee for Standardization, Brussels (2013)

Grenet, L.: Mechanical strength of glass. Bulletin de la Société d'Encouragement pour l'Industrie Nationale **5**(4), 838–848 (1899)

Gy, R.: Stress corrosion of silicate glass: review. J. Non Cryst. Solids **316**, 1–11 (2003)

Haldimann, M.: Fracture Strength of Structural Glass Elements—Analytical and Numerical Modelling, Testing and Design. École Polytechnique Fédérale de Lausanne, Lausanne (2006)

Haldimann, M., Luible, A., Overend, M.: Structural Use of Glass. International Association for Bridge and Structural Engineering IABSE, Zurich (2008)

Jotz, M., Schneider, J., Radlein, E.: Introducing the "Cylinder Fit Test", a simplified edge strength measurement method for ultra thin glass. In: Schneider, J., Weller, B. (eds.) Engineered Transparency 2018—Glass in Architecture and Structural Engineering, pp. 65–73. Wilhelm Ernst & Sohn, Berlin (2018)

Kinsella, D., Persson, K.: A numerical method for analysis of fracture statistics of glass and simulations of a double ring bending test. Glass Struct. Eng. **3**, 139–152 (2018)

Kurkjian, C.R., Simpkins, P.G., Inniss, D.: Strength, degradation, and coating of silica lightguides. Glass Sci. Technol. **76**, 1106–1112 (1993)

Lawn, B.: Fracture of Brittle Solids, 2nd edn. Cambridge University Press, Cambridge (1993)

Le Bourhis, E.: Glass—Mechanics and Technology. Wiley-VHC, Weinheim (2014)

Lindqvist, M., Louter, C., Lebet, J.P.: Edge-strengthening of structural glass with protective coatings. Key Eng. Mater. **488–489**, 331–334 (2012)

Michalske, T.A.: Fractography of slow fracture in glass. In: Mecholsky, J.J., Powell, S.R. (eds) Fractography of Ceramic and Metal Failures. American society for testing and materials - ASTM STP 827, pp. 121–136 (1984)

Michalske, T.A., Freiman, S.W.: A molecular mechanism for stress corrosion in vitreous silica. J. Am. Ceram. Soc. **66**, 284–288 (1983)

Michalske, T.A., Fréchette, V.D., Hudson, R.: Dynamic effects of liquids on surface crack extension in glass. In: Francis, D. (ed.) Advances in Fracture Research, vol. 2, pp. 1091–1097. Pergamon, New York (1981)

Overend, M., Louter, C.: The effectiveness of resin-based repairs on the inert strength recovery of glass. Constr. Build. Mater. **85**, 165–174 (2015)

Overend, M., Zammit, K.: A computer algorithm for determining the tensile strength of float glass. Eng. Struct. **45**, 68–77 (2012)

Overend, M., De Gaetano, S., Haldimann, M.: Diagnostic interpretation of glass failure. Struct. Eng. Int. **17**, 151–158 (2007)

Pisano, G., Royer Carfagni, G.: The statistical interpretation of the strength of float glass for structural applications. Constr. Build. Mater. **98**, 741–756 (2015)

Quinn, G.: Fractography of Ceramics and Glasses, 2nd edn. National Institute of Standards and Technology, Gaithersburg (2016)

Ronchetti, C., Lindqvist, M., Louter, C., Salerno, G.: Stress-corrosion failure mechanisms in soda-lime silica glass. Eng. Fail. Anal. **35**, 427–438 (2013)

Vitale, A., Priola, A., Tonelli, C., Bongiovanni, R.: Nanoheterogeneous networks by photopolymerization of perfluoropolyethers and acrylic co-monomers. Polym. Int. **62**, 1395–1401 (2013)

Vitale, A., Bongiovanni, R., Ameduri, B.: Fluorinated oligomers and polymers in photopolymerization. Chem. Rev. **115**, 8835–8866 (2015)

Wang, B., Cunning, B.V., Park, S.Y., Huang, M., Kim, J.Y., Ruoff, R.S.: Graphene coatings as barrier layers to prevent the water-induced corrosion of silicate glass. ACS Nano **10**, 9794–9800 (2016)

Wiederhorn, S.M.: Influence of water vapor on crack propagation in soda-lime glass. J. Am. Ceram. Soc. **50**, 407–414 (1967)

Wiederhorn, S.M., Bolz, L.H.: Stress corrosion and static fatigue of glass. J. Am. Ceram. Soc. **53**, 543–548 (1967)